Neuro-Oncology
26(1), 100–114, 2024 | https://doi.org/10.1093/neuonc/noad159 | Advance Access date 31 August 2023

EPIC-1042 as a potent PTRF/Cavin1–caveolin-1 interaction inhibitor to induce PARP1 autophagic degradation and suppress temozolomide efflux for glioblastoma

Biao Hong†, Eryan Yang†, Dongyuan Su†, Jiasheng Ju, Xiaoteng Cui, Qixue Wang, Fei Tong, Jixing Zhao, Shixue Yang, Chunchao Cheng, Lei Xin, Menglin Xiao, Kaikai Yi, Qi Zhan, Yaqing Ding, Hanyi Xu, Longtao Cui, and Chunsheng Kang

All author affiliations are listed at the end of the article

Corresponding Author: Chunsheng Kang, PhD, Tianjin Medical University General Hospital, 154 Anshan Road, Tianjin 300052, China (kang97061@tmu.edu.cn)

†These authors contributed equally to this work.

Abstract

Background. Temozolomide (TMZ) treatment efficacy in glioblastoma is determined by various mechanisms such as TMZ efflux, autophagy, base excision repair (BER) pathway, and the level of O^6-methylguanine-DNA methyltransferase (MGMT). Here, we reported a novel small-molecular inhibitor (SMI) EPIC-1042 ($C_{20}H_{28}N_6$) with the potential to decrease TMZ efflux and promote PARP1 degradation via autolysosomes in the early stage.

Methods. EPIC-1042 was obtained from receptor-based virtual screening. Co-immunoprecipitation and pull-down assays were applied to verify the blocking effect of EPIC-1042. Western blotting, co-immunoprecipitation, and immunofluorescence were used to elucidate the underlying mechanisms of EPIC-1042. *In vivo* experiments were performed to verify the efficacy of EPIC-1042 in sensitizing glioblastoma cells to TMZ.

Results. EPIC-1042 physically interrupted the interaction of PTRF/Cavin1 and caveolin-1, leading to reduced secretion of small extracellular vesicles (sEVs) to decrease TMZ efflux. It also induced PARP1 autophagic degradation via increased p62 expression that more p62 bound to PARP1 and specially promoted PARP1 translocation into autolysosomes for degradation in the early stage. Moreover, EPIC-1042 inhibited autophagy flux at last. The application of EPIC-1042 enhanced TMZ efficacy in glioblastoma *in vivo*.

Conclusion. EPIC-1042 reinforced the effect of TMZ by preventing TMZ efflux, inducing PARP1 degradation via autolysosomes to perturb the BER pathway and recruitment of MGMT, and inhibiting autophagy flux in the later stage. Therefore, this study provided a novel therapeutic strategy using the combination of TMZ with EPIC-1042 for glioblastoma treatment.

Key Points

- EPIC-1042 prevented temozolomide efflux by inhibiting small extracellular vesicles secretion.
- EPIC-1042 induced PARP1 autophagic degradation mediated by increased binding of p62 to PARP1.
- EPIC-1042 inhibited autophagy flux in the later stage.

Graphical Abstract

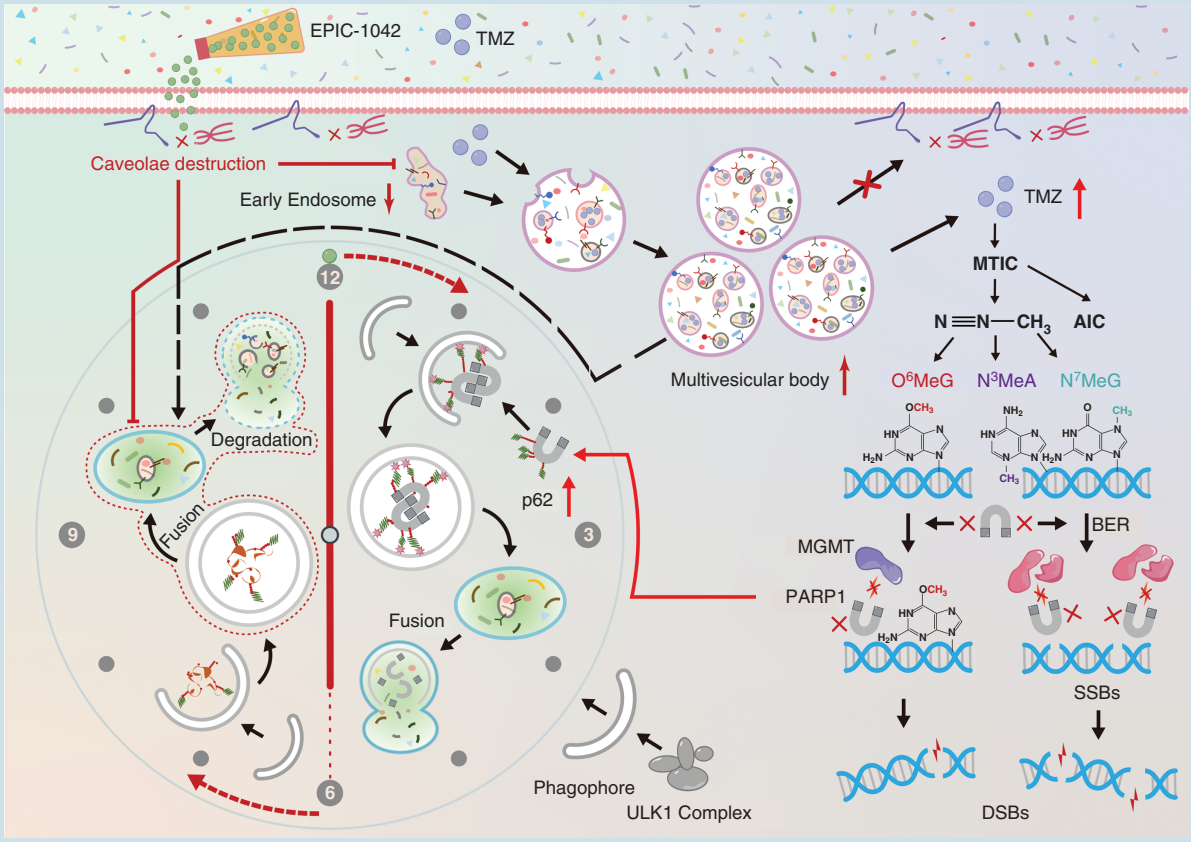

Importance of the Study

Reversing temozolomide (TMZ) chemoresistance to enhance TMZ efficacy is in urgent need in the treatment of glioblastoma. It is, therefore, essential to unveil the underlying mechanisms of TMZ resistance and explore potent therapeutic strategies. Here, we reported on a SMI, EPIC-1042, which selectively interrupted the binding of PTRF/Cavin1 with caveolin-1 and suppressed TMZ efflux by inhibiting the secretion of sEVs. Furthermore, EPIC-1042 induced autophagic degradation of PARP1 through increased binding of p62 to PARP1 in the early stage, generating suppressed BER pathway and MGMT recruiting to prevent repair of TMZ-methylated adducts. It also inhibited autophagy flux ultimately. Consequently, EPIC-1042 showed a synergistic effect with TMZ both *in vitro* and *in vivo*, suggesting that combining EPIC-1042 and TMZ could be an improved anti-glioblastoma regimen.

Genomic instability is a pathological hallmark of cancer cells, resulting from abnormal DNA damage response (DDR) signaling.[1] Dysregulated DDR can act as a double-edged sword in carcinogenesis by altering the genomic stability on the one hand, and being exploited with both conventional cytotoxic therapy and DDR inhibitors on the other hand. Therefore, DDR pathway-targeted inhibitors have been developed to overcome the clinical challenges of chemoresistance and to reinforce the efficacy of conventional chemotherapeutics.[2]

Glioblastoma (GBM) is the most aggressive primary brain malignancy that exhibits disproportionate morbidity and mortality rates with a 5-year survival of 6.8%.[3] Because of efficient blood–brain barrier (BBB) penetration capacity, TMZ is used as the first-line medication for GBM treatment.[4] N^7-methylguanine (N^7MeG) and N^3-methyladenine (N^3MeA) are the majority of TMZ-methylated nucleotides, accounting for 70% and 9%, respectively, and are efficiently removed by the base excision repair (BER) pathway in which PARP1 plays a key role. While O^6-methylguanine (O^6MeG) adducts, contributing to about 5% of alkylated DNA products, lead to persistent DNA damage in MGMT-deficient cancer cells.[1] However, the development of TMZ resistance and sudden relapse-associated death upon long-term therapy has been a serious roadblock in GBM treatment.

Importantly, a new era of drug discovery has been rapidly emerging where high-efficiency and minimally cytotoxic small molecule inhibitors (SMIs) are being developed by computer-aided drug design (CADD) and machine learning (ML) to cure GBM.[5,6] Evidence supports that PARP1 deficiency impairing the BER pathway not only decreases the level of PARylation but also increases TMZ sensitivity in chordoma cells.[7,8] Therefore, CADD-guided designing of novel SMIs against the BER pathway and/or MGMT expression directly or indirectly is likely to enhance the efficacy of TMZ treatment.

Caveolae, nanoscale (60–80 nm) cup-shaped invaginations of the plasma membrane, are identified by the presence of caveolin proteins and play important roles in endocytosis, cholesterol and lipid metabolism, and cellular signaling. Compared to the other members in the caveolin family, caveolin-1 (CAV1) driving caveolae formation is the caveolae's major constituent and expresses in various tissues.[9–11] Moreover, Polymerase I and Transcript Release Factor (PTRF), also called Cavin1, recruitment to the plasma membrane by CAV1 with the existence of cholesterol and phosphatidylserine (PS) is crucial for the genesis and functionality of caveolae.[9] We have shown that the PTRF-CAV1 complex can be loaded into small extracellular vesicles (sEVs) in a caveolae-related way and takes part in sEVs genesis, traffic, and secretion. Furthermore, increased binding between PTRF and CAV1 can increase caveolae and promote sEVs production and uptake.[12] Interestingly, sEVs could be exploited as carriers for transfer of membrane-embedded drug efflux pumps and for the efflux of anticancer therapeutics.[13] We have also revealed that PTRF knockout (KO) inhibits the PTRF-CAV1 complexation, caveolae formation, and sEVs production, as well, which in turn elevates intracellular TMZ concentration in GBM cells.[14] In summary, disrupting the interaction between PTRF and CAV1 could be a promising therapeutic approach to enhance TMZ efficacy.

Autophagy is an active process of the degradation of damaged proteins and organelles and the recycling of their components. Thus, it acts as one of the important protective mechanisms against stress.[15,16] Emerging evidence suggests that TMZ treatment can induce autophagy to support elevated intracellular demands of energy and resources for survival, which contributes to TMZ resistance in GBM. Furthermore, treatments with a combination of chloroquine diphosphate (CQ), ATG4B inhibitor, or ATG5 knockdown (KD) have been shown to suppress autophagy and enhance TMZ efficacy in GBM.[4,16,17] P62, a classical autophagy receptor, utilizes its C-terminal ubiquitin-associated (UBA) domain to interact with ubiquitinated cargos as well as LC3-interacting region (LIR) to bind with microtubule-associated protein 1 light chain 3-II (LC3-II) to tether the cargos to the inner membrane of autophagosomes for degradation.[15] Notably, p62 can selectively regulate the turnover of PD-L1 in lung cancer treated by Sunitinib.[18] Also, several other studies have implicated the crucial roles of PTRF and CAV1 in the regulation of autophagy.[19,20] However, whether the interaction between PTRF and CAV1 crucial for caveolae formation can influence autophagy remains unclear.

In this study, we examined the potential of EPIC-1042 to disrupt the interaction between PTRF and CAV1 and enhance TMZ sensitivity in GBM cells though inhibiting sEVs secretion to increase intracellular concentration of TMZ, promoting PARP1 autophagic degradation by increased binding of p62 to PARP1 in the early stage and suppressing autophagy flux in the later stage. This study provided a novel therapeutic strategy by combining EPIC-1042 and TMZ in treating GBM.

Materials and Methods

Pull-Down of EPIC-1042-Biotin

Cells were lysed in NP-40 (Beyotime) with 1% PMSF and centrifuged. Then, the supernatant was collected, equally divided into 3 tubes, and incubated with DMSO, 100 μmol/l EPIC-1042, and 100 μmol/l EPIC-1042-Biotin overnight at 4°C, respectively. Next, the samples were incubated with streptavidin magnetic beads (Beyotime) at 4°C for 4 h, then the beads were washed 3 times for a total time of 15 min. Finally, pull-downed samples were analyzed by WB.

In Vivo Xenograft Mouse Models

All animal study protocols were approved by the Institutional Animal Care and Use Committee (IACUC) of Tianjin Medical University (No. IRB2022-DWFL-069). Four-week-old female BALB/c nude mice were used to construct an orthotopic GBM model and a subcutaneous model. See Supplementary Materials for details.

Statistical Analysis

GraphPad Prism 8.4.0 software was used to perform all statistical analyses and outcome graphs. For functional analysis, Student's *t*-test or analysis of variance (ANOVA) was utilized. The combination score was measured by SynergyFinder (Bliss Model)[21] Error bars implied the mean ± standard deviation (SD) for the results obtained from at least 3 independent experiments. Significances were defined as $*P < 0.05$, $**P < 0.01$, $***P < 0.001$, and $****P < 0.0001$, and n.s. indicated no significant difference.

Other Methods

For materials and methods related to cells culture and drugs, protein extraction, western blotting (WB), immunofluorescence (IF) assay, cell viability and clonogenic assays, co-immunoprecipitation (Co-IP), transmission electron microscopy (TEM), sEVs isolation and characterization, LC-MS samples preparation, hematoxylin and eosin (H&E) staining, immunohistochemistry (IHC), RNA isolation, quantitative real-time PCR (qRT-PCR), siRNA transfection and lentiviral transduction, see Supplementary Materials for details.

Results

Receptor-Based Virtual Screening for EPIC-1042 to Inhibit PTRF-CAV1 Interaction

In our published study, through homology modeling, interaction patterns prediction, and molecular dynamic simulation, we exhibited a transmembrane RTRF-CAV1 complex (Figure 1A).[12] Importantly, we identified 2 essential amino

acid (aa) residues of PTRF, Glu10 of chainA and Arg11 of chainC with dihydrogen bonds for Ser9 - Lys26 and Gly22 of CAV1, respectively, thereby strengthening the association between these 2 proteins (Figure 1A). We also performed an alignment analysis of PTRF protein sequences from 28 mammalian species. The result indicated that Glu10 and Arg11 residues were highly conserved across the species (Supplementary Figure S1A) and thus could be exploited for SMI-based targeted intervention. Then, we constructed 2 forms of docking grids, grid 1 with CAV1 and grid 2 without CAV1, to simulate the replacement of CAV1 into PTRF and the environment provided by a free PTRF. Finally, RBVS analyses were carried out to screen for potential candidates with high docking scores in both grids, and 15 compounds were identified (Supplementary Figure S1B), and their IC_{50} values were determined in TBD-0220. Interestingly, EPIC-1042 showed the lowest IC_{50} value of 38.00 μM (Supplementary Figure S1C) and the molecular simulation and docking analysis were illustrated in Figure 1B and Supplementary Figure S1D. We found that EPIC-1042 interacted with Glu10 of chain A. Furthermore, the anticancer efficacy of EPIC-1042 was tested in other GBM cell lines, U87-MG and LN229, as well (Supplementary Figure S1E).

Next, we evaluated whether EPIC-1042 could block the mutual binding of PTRF and CAV1 effectively. PTRF-eGFP was transduced into GBM cell lines via lentivirus, which was confirmed by WB (Supplementary Figure S2A). Besides, we conjugated EPIC-1042 with Biotin (E-Biotin) to verify whether EPIC-1042 could combine to PTRF (Supplementary Figure S2B). The results showed that not only endogenous PTRF but also ectopically expressed PTRF-eGFP were strongly pulled down by streptavidin magnetic beads after E-Biotin treatment, while no signal was detected in non-biotinylated EPIC-1042 groups, suggesting the biotin-streptavidin interaction specificity (Figure 1C). Furthermore, we performed Co-IP assays using an anti-PTRF antibody and found that CAV1 bound to PTRF and PTRF-eGFP was hardly detected after EPIC-1042 treatment, compared with DMSO treatment (Figure 1D). Notably, we found that EPIC-1042 treatment did not affect expressions of PTRF and CAV1 in GBM cells. IF analysis also implied the same results with decreased colocalization coefficient of PTRF-eGFP and CAV1 in LN229 cell line and the number of caveolae also decreased in U87-MG cells (Supplementary Figure S2C–F) after EPIC-1042 treatment. Collectively, EPIC-1042 could potentially block the PTRF-CAV1 interaction with high docking scores and the best proliferation inhibition.

EPIC-1042 Inhibits sEVs Secretion and Increases Intracellular TMZ Concentration

Practically, exosomes are hard to isolate in complete purity; hence, we utilized the term "sEVs" to refer to pellets obtained from ultracentrifugation (100,000 g, classically considered as exosomes) from conditioned medium. To analyze the impact of EPIC-1042 on different subtypes of EVs, pellets were sequentially collected at 2,000 g (2K pellet), 10,000 g (10K pellet) and 100,000 g (sEVs) from GBM cell lines for further analysis.

First, we quantified the total protein content in each of the pellets, revealing a significant decrease only in sEVs after EPIC-1042 treatment (Figure 1E, Supplementary Figure S2G–H). To further profile different subtypes, universally characterized exosome markers were analyzed by WB in different pellets as well as in whole cell lysates (WCLs) (Figure 1F, Supplementary Figure S2I), showing a significant presence of Alix, CD63, Tsg101, and CD9 in all samples. However, calnexin, the exosome-excluded endoplasmic reticulum (ER) protein, was rarely detected in ultracentrifuged sEVs but was prominently detected in both 2K, 10K pellets and WCLs, suggesting that exosomes in sEVs were highly pure. As EVs were centrifuged from an equal number of cells, the intensity of the exosome markers reflected the population of EVs. EPIC-1042 treatment decreased the quantity of Alix, Tsg101, and CD9 markers in sEVs but not in the WCL. Moreover, CD63, also a marker of multivesicular bodies (MVBs) directly giving rise to exosomes, showed the same trend (Figure 1F, Supplementary Figure S2J). These results suggest that EPIC-1042 treatment might have impaired the secretion of sEVs instead of affecting the expression of marker proteins. However, there were no significant differences in the contents of exosome-specific proteins in 2K and 10K pellets compared to DMSO (Supplementary Figure S2I). Taken together, EPIC-1042 could specifically inhibit the secretion of sEVs by disrupting the interaction between PTRF and CAV1.

Furthermore, the Nanosight analysis of ultracentrifuged pellets consistently showed a significant decrease in the number of particles after treatment of EPIC-1042 and that EPIC-1042 did not result in a mere reduction in ultracentrifuged pellets but an actual reduction in sEVs (Figure 1G–H). Moreover, the majority of ultracentrifuged EVs, isolated from EPIC-1042-treated cells, exhibited similar size compared to that from DMSO-treated cells. Next, as we expected, a combination regimen of TMZ and EPIC-1042 showed intracellular TMZ concentration determined by LC-MS approximately twice the amount in TMZ alone treated TBD-0220 cells and TMZ concentration in sEVs derived from EPIC-1042+TMZ-treated cells decreased compared to that in sEVs generated from TMZ-treated cells (Figure 1I and Supplementary Figure S3A–B), suggesting EPIC-1042 could inhibit sEVs-mediated TMZ efflux. Finally, we used CRISPR-Cas9 gene editing system to knockout PTRF to confirm the specificity of EPIC-1042 to PTRF. The qualification of sEVs' total protein, exosome markers, and the Nanosight analysis of sEVs showed no significant change in EPIC-1042-treated PTRF-KO cells and their sEVs compared to the DMSO-treated PTRF-KO cells and their sEVs (Supplementary Figure S3C–G).

EPIC-1042 Inhibits Autophagy Flux

We observed that EPIC-1042 could abnormally accumulate MVBs (Figure 1F, Supplementary Figure S2J). As MVBs originates from inward invagination of the early endosome membrane, the elevated MVBs could be attributed to either an increase in the MVB biogenesis or a decrease in MVB transport and degradation (Supplementary Figure S10A). Hence, first, the early endosome marker

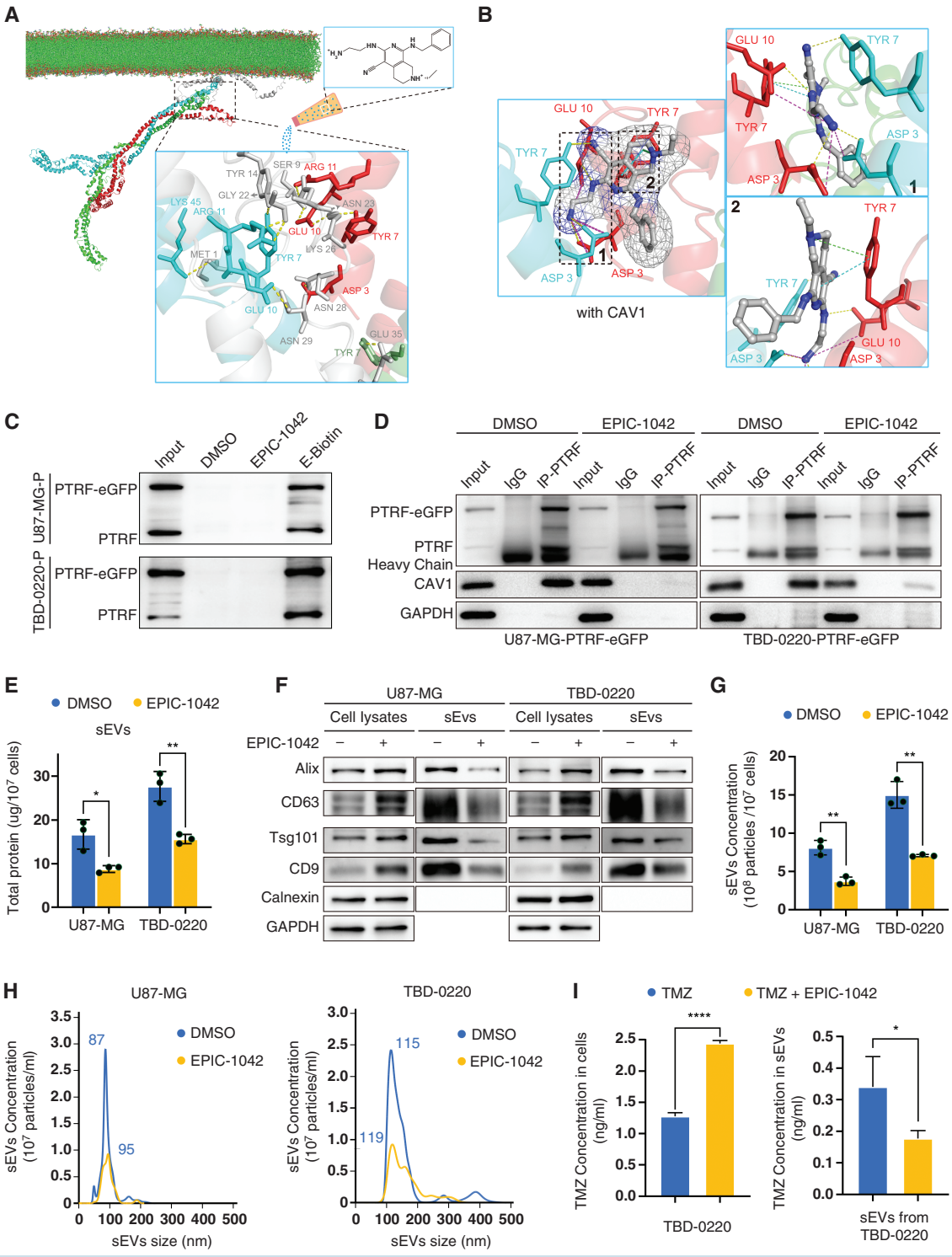

Figure 1. Development of EPIC-1042 to inhibit PTRF-CAV1 interaction and sEVs secretion to increase intracellular TMZ concentration. (A) Molecular dynamics simulation of PTRF-CAV1 complex. The proteins stained with red, green, cyan, and gray indicate chain A, chain B, and chain C of PTRF as well as CAV1, respectively. (B) Molecular simulation of the interaction between EPIC-1042 and PTRF in docking grid1 with CAV1. (C) Pull-down of cell lysates treated with DMSO, EPIC-1042 (100 μM), and E-Biotin (100 μM) for 24 h. (D) Co-IP assays were conducted with anti-PTRF antibody in PTRF-eGFP cells. (E) Total protein levels of sEVs secreted by equal number of GBM cells. (F) WB analysis of exosome markers in whole cell lysates and sEVs from equal number of GBM cells. (G–H) Quantification and traces of Nanosight analysis for sEVs derived from equal number of GBM cells. (I) Quantification of concentrations of TMZ in equal TMZ (100 μM)- or TMZ (100 μM) +EPIC-1042 (20 μM)- treated cells and in sEVs from equal number of treated cells. In D–H, cells were treated with DMSO or 20 μM of EPIC-1042 for 48 h. Error bars represent mean ± SD; $n = 3$ independent experiments. $^{*}P < 0.05$, $^{**}P < 0.01$ and $^{****}P < 0.0001$.

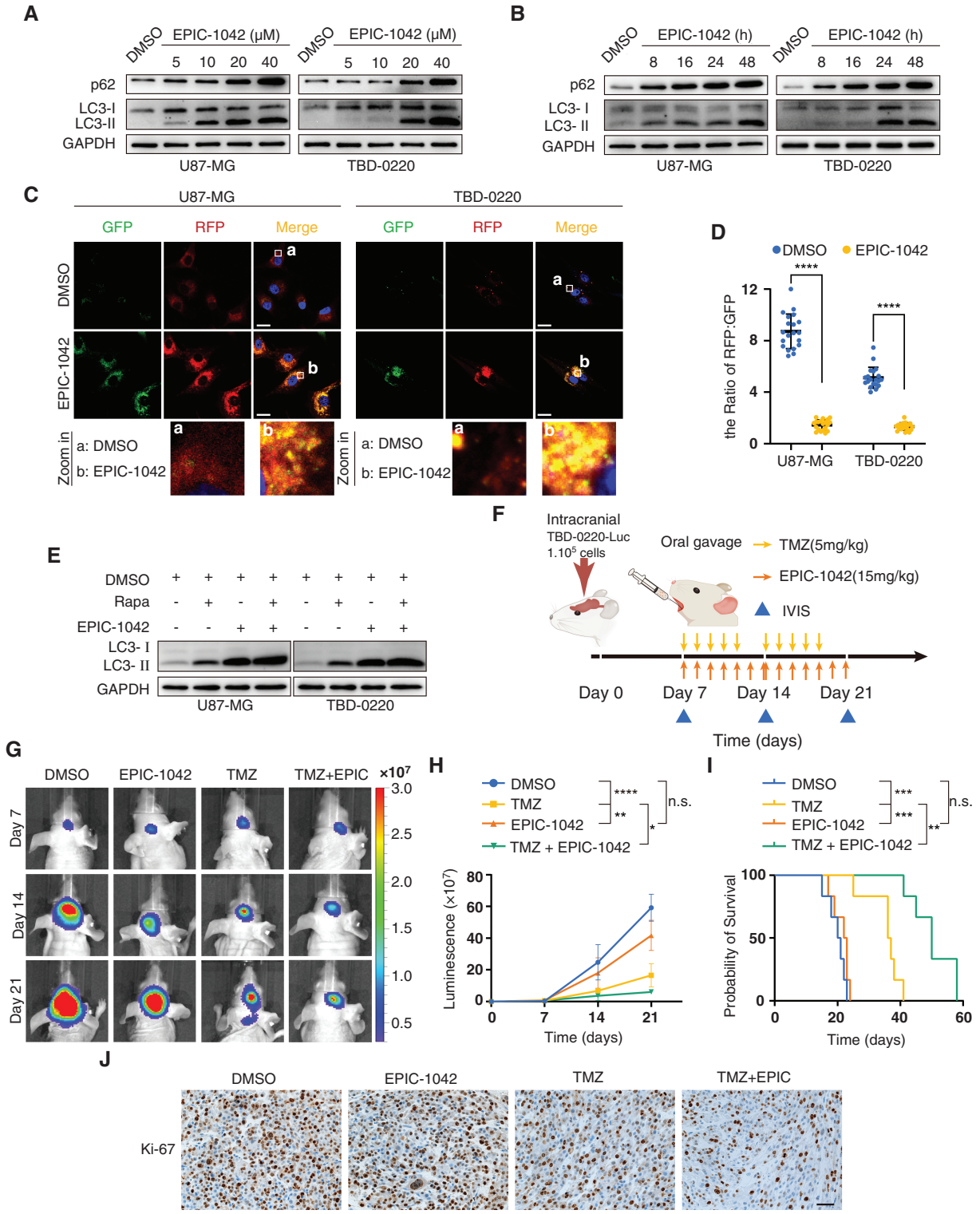

Figure 2. EPIC-1042 inhibits autophagy flux and increase TMZ sensitivity *in vivo*. (A–B) WB analysis of p62 and LC3 in GBM cells treated with indicated concentrations of EPIC-1042 for 48 h or 20 μM of EPIC-1042 for indicated hours. (C–D) IF images of LC3-RFP-GPF and the ratio of LC3-RFP: LC3-GFP in cells treated with DMSO or 20 μM of EPIC-1042 for 48 h, $n = 20$. Scale bar, 20 μm. (E) WB analysis of LC3 in cells treated with DMSO, 20 μM of EPIC-1042, 25 nM of Rapamycin, or combination for 48 h. (F) Tumor-bearing nude mice were treated with DMSO, TMZ (5 mg/kg), EPIC-1042 (15 mg/kg), or TMZ (5 mg/kg) + EPIC-1042 (15 mg/kg) by gavage for 2 weeks, $n = 6$ for each group. (G–H) Bioluminescence images from representative mice and quantification of bioluminescence intensity of all groups. *P*, two-way ANOVA. (I) Kaplan–Meier survival curve of nude mice. *P*, Log-rank test. (J) Ki-67 level in tumor tissues of all groups. Scale bar, 40 μm. Error bars represent mean ± SD; $n = 3$ independent experiments. $^{*}P < 0.05$, $^{**}P < 0.01$, $^{***}P < 0.001$, $^{****}P < 0.0001$, and n.s. indicated no significant difference.

early endosome antigen 1 (EEA1) showed a decreasing trend in a dose- and time-dependent manner after EPIC-1042 treatment, which was also confirmed by IF analysis (Supplementary Figure S4A–C). However, there were no significant differences in EEA1 subcellular distribution patterns. The fusion of MVBs with autophagosomes to form amphisomes for degradation is the converging point of endocytosis and autophagy.[22] Besides, methyl-β-cyclodextrin (MBCD)-mediated depletion of membrane-bound cholesterol and disruption of lipid rafts have been shown to induce autophagy in mouse embryonic fibroblasts,[20] and the caveola is one kind of lipid raft. Therefore, we sought to test the effect of EPIC-1042 on autophagy. We found that EPIC-1042 increased p62 and autophagosome marker LC3-II levels in a time- and dose-dependent manner by WB (Figure 2A–B). An increase in LC3-II level could be either due to the induction of autophagosomes formation or inhibition of protein degradation. To distinguish between these 2 likelihoods, we first characterized key genes that were known to play important roles in the maturation of autophagosomes. We observed that the total protein levels of these genes remained unaltered after EPIC-1042 treatment which ruled out the induction of autophagy (Supplementary Figure S4D). Next, we revealed the autophagic flux by confocal imaging in GBM cell lines ectopically expressing dual-tagged (GFP and RFP) LC3 in such a way that lysosomal acidic condition would quench GFP fluorescence but not RFP, and the ratio of RFP to GFP fluorescence could be used to evaluate autophagic flux. IF imaging showed that the RFP puncta were increased by EPIC-1042 exposure, corresponding to WB analysis. However, the RFP:GFP ratio was drastically reduced when assessed at 48 hours post EPIC-1042 treatment (Figure 2C–D). Collectively, these results suggested that EPIC-1042 can significantly inhibit the autophagic degradation of proteins without affecting the genesis of autophagosomes. These results also confirmed that MVBs generating exosomes were indeed increased. To further verify these effects of EPIC-1042, GBM cells were treated with Rapamycin, an MTOR inhibitor that could induce autophagy, and EPIC-1042 in combination or individually, which showed that the cotreatment induced a higher level of LC3-II than Rapamycin alone, thus excluding the possibility that EPIC-1042 promoted autophagosomes development (Figure 2E, Supplementary Figure S4E). Finally, we demonstrated that EPIC-1042 could modulate TMZ-induced autophagy by blocking autophagic degradation to further increase the LC3-II level in GBM cells (Supplementary Figure S4F).

EPIC-1042 Enhances TMZ Efficacy in MGMT-Deficient GBM Tumors *In Vivo*

As stated earlier, we established an intracranial xenografts nude mouse model by utilizing TBD-0220 cells to test EPIC-1042's potential to enhance TMZ efficacy (Figure 2F). While EPIC-1042 alone could slightly suppress the tumor growth without significance compared with DMSO, combination with TMZ showed the highest level of reduction in tumor burden among the 4 treatment groups by luminescence intensity measurement (Figure 2G–H). Furthermore, EPIC-1042 monotherapy did not present any overall survival (OS) benefit, however, it enhanced the efficacy of TMZ in combination therapy (Figure 2I, Supplementary Figure S4G). The median survival of the combination therapy group was about 1.5 times higher than that of the TMZ monotherapy group. H&E staining of brain tumor sections indicated an enhanced treatment efficacy with the smallest tumor size in the combination therapy group compared to monotherapy groups, which was further supported by the IHC analysis using an anti-Ki-67 antibody (Supplementary Figure S4H, Figure 2J). Taken together, our results demonstrated that EPIC-1042 could enhance TMZ efficacy *in vivo*.

EPIC-1042 Induces p62-Mediated PARP1 Degradation by Selective Autophagy in the Early Stage

Based on the *in vivo* cotherapeutic effects, we speculated that there might be additional underlying mechanisms regulating TMZ efficacy. EPIC-1042 could not influence on MGMT to increase the amount of O^6MeG in TBD-0220 and U87-MG cells. However, N^3MeA and N^7MeG leading to cytotoxicity could be increased by perturbing BER pathway, and PARP1's lacking could impair the BER pathway. Interestingly, we found that the total PARP1 protein level was decreased after EPIC-1042 treatment (Figure 3A). While *PARP1* mRNA level remained unchanged (Supplementary Figure S5A), suggesting that EPIC-1042 induced PARP1 protein degradation. To verify that, GBM cells were treated with either protein synthesis inhibitor cycloheximide (CHX) or CHX+EPIC-1042 in a time-dependent manner. WB showed that PARP1 degradation occurred faster in combination treatment than that in CHX alone treatment (Figure 3B–C). Given that the autophagy and ubiquitin-proteasome system (UPS) are the main proteolytic systems, we aimed to distinguish the one that might contribute to the PARP1 protein level regulation. Hence, we treated TBD-0220 and U87-MG cell lines with lysosomal inhibitor CQ, proteasome inhibitor MG132, CHX, or EPIC-1042 for 16 and 24 hours, respectively. PARP1 was vastly degraded treated with CHX alone, and this effect could be rescued by MG132 but not CQ. Dual therapy of EPIC-1042 and CHX further enhanced the degradation of PARP1 compared to the CHX monotherapy, however, this effect could be reverted by both MG132 and CQ (Figure 3D). These results indicated that, under normal conditions, PARP1 was degraded only by UPS, while EPIC-1042 further induced PARP1 degradation by autophagy, implying a novel regulatory role of EPIC-1042 in PARP1 turnover.

We observed that in the early stage of EPIC-1042 treatment (0-24 hours in U87-MG and 0-16 hours in TBD-0220), EPIC-1042 cannot increase LC3-II level significantly but substantially elevated the p62 level (Figure 3E and Supplementary Figure S5B). The accelerated degradation of PARP1 also occurred during the same time course in 2 cell lines (Figure 3C). Besides, IF imaging showed that the autophagy flux maintained a steady state after 16 and 24 hours of EPIC-1042 treatment in TBD-0220 and U87-MG cells, respectively (Supplementary Figure S5C–D). These outcomes reminded us that p62 might mediate autophagic degradation of PARP1, but we cannot exclude the possibility that UPS was not involved in the accelerated

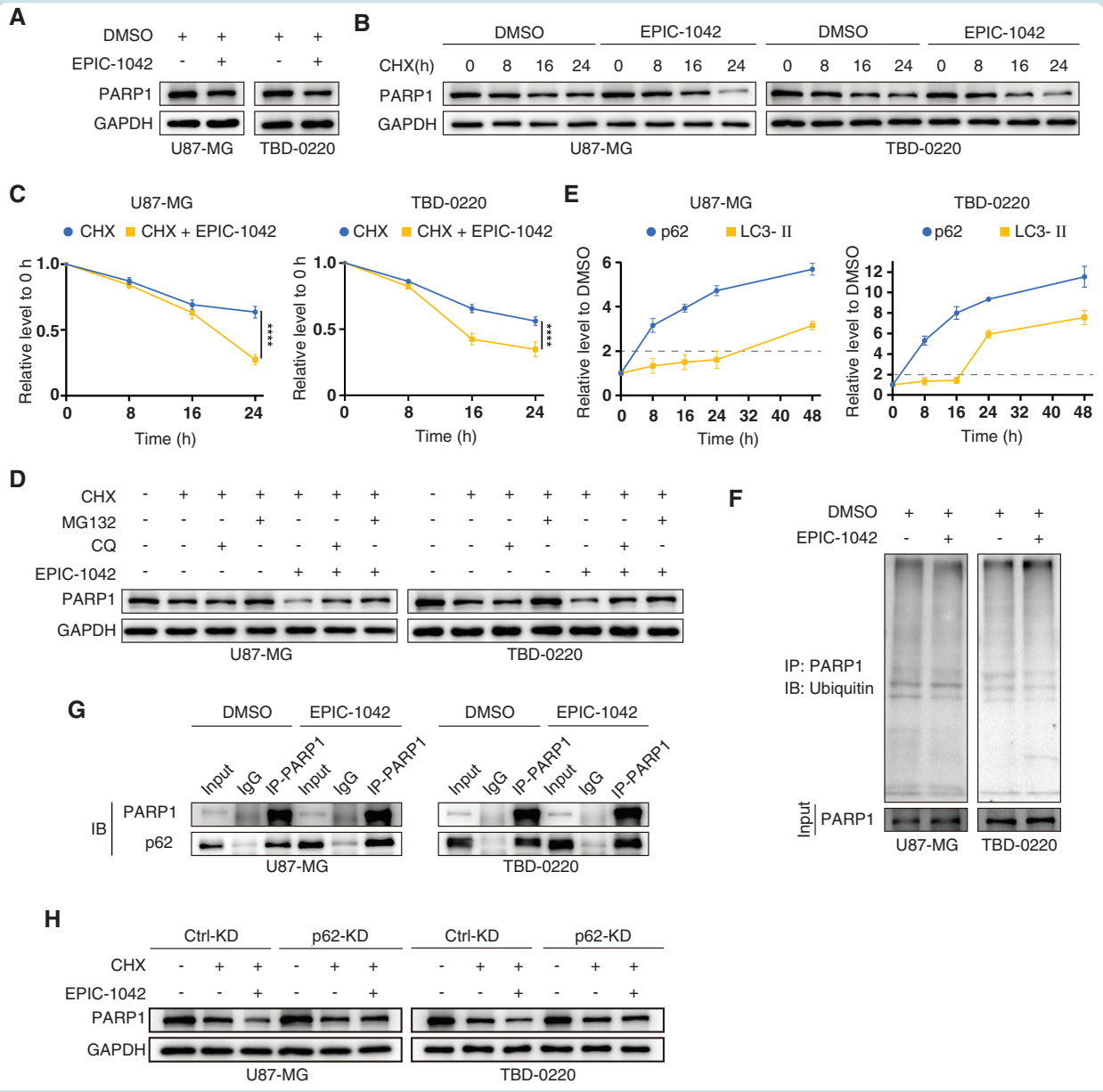

Figure 3. EPIC-1042 induces p62-mediated autophagic PARP1 degradation. (A) Protein level of PARP1 in cells treated with DMSO or 20 μM of EPIC-1042 for 48 h. (B–C) WB analysis and quantification of PARP1 degradation in cells treated with CHX or combination of CHX with 20 μM of EPIC-1042 for 24 h. (D) WB analysis of PARP1 in U87-MG and TBD-0220 cells treated with CHX, MG132, CQ, or 20 μM of EPIC-1042 for 24 and 16 h, respectively. (E) Quantification of p62 and LC3-II levels in a time-dependent manner in Figure 2B. (F–G) Co-IP assays were conducted with anti-PARP1 antibody in U87-MG and TBD-0220 cells treated with DMSO or 20 μM of EPIC-1042 for 16 and 8 h, respectively, followed by immunoblotting with ubiquitin and p62. (H) WB analysis of PARP1 in Ctrl-KD- and p62-KD-U87-MG and TBD-0220 cells treated with CHX or combination of CHX with 20 μM of EPIC-1042 for 24 and 16 h, respectively. Error bars represent mean ± SD; $n = 3$ independent experiments. ****$P < 0.0001$.

degradation of PARP1. To verify our conjecture, we performed Co-IP assays using anti-PARP1 antibody. TBD-0220 and U87-MG cell pellets were collected after 8 and 16 hours post EPIC-1042 exposure, respectively, before PARP1 was degraded enormously. As shown in Figure 3F–G, the ubiquitinated PARP1 level remained unchanged but PARP1's binding with p62 significantly increased, suggesting a prompt induction of PARP1 loading into autophagosomes for degradation. To further test that decreased stability of PARP1 was due to p62-related autophagy, we performed siRNA-mediated knockdown (KD) of *p62* in TBD-0220 and U87-MG cells (Supplementary Figure S5E) and treated them with CHX or CHX+EPIC-1042 for 16 and 24 hours, respectively. We found that p62 KD did not affect PARP1 level compared to the Ctrl-KD group, which also implied that pre-existing p62 did not mediate autophagic degradation of PARP1. As we expected, in p62-KD group, no additional PARP1 degradation was observed with the combination treatment compared to CHX monotherapy (Figure 3H). Notably, we also observed that the UPS was the only mode

of PARP1 degradation in the p62-KD cells after treatment of EPIC-1042 (Supplementary Figure S5F). These results indicated that increased p62 binding was vital for selective autophagic degradation of PARP1 following EPIC-1042 treatment, which enhanced TMZ efficacy.

EPIC-1042 Enhances TMZ Sensitivity in MGMT-Positive GBM

Cytotoxic O^6MeG would be readily repaired by MGMT, contributing chemoresistance to TMZ. PARP1 recruits MGMT to sites of DNA damage and poly(ADP)ribosylates MGMT to promote the repair of O^6MeG.[23] Hence, MGMT-positive T98G and LN-18 GBM cells were utilized to assess the effect of EPIC-1042 on their sensitivities to TMZ. We found that EPIC-1042 had no influence on MGMT turnover in 24 hours of treatment (Supplementary Figure S6A); given that MGMT degradation is mediated by UPS under normal conditions,[24] hence, EPIC-1042 could not effect MGMT stability whatever by increased p62 or inhibition of autophagy flux. But EPIC-1042 could also reduce PARP1 level in these lines (Figure 4A). We measured MGMT activity through O^6MeG removal kinetics by IF showing that TMZ alone induced weak O^6MeG increase; however, the combination treatment significantly elevated the O^6MeG accumulation (Figure 4B), and the PARP1 level in different groups was shown in Supplementary Figure S6B. These outcomes indicated that the declining ability of MGMT in removing O^6MeG was impacted by reduced PARP1 level. The intracellular level of γ-H2AX showed the same trend as O^6MeG in both WB and IF analyses (Figure 4C–D). In addition, the dose-response matrix outcomes also indicated a synergistic efficacy of TMZ with EPIC-1042 and proliferation rates of both cell lines were significantly inhibited by the combination treatment (Figure 4E and Supplementary Figure S6C–D). Furthermore, we downregulated p62 to prevent PARP1 degradation in T98G and LN-18 cell lines using siRNA against *p62* (Supplementary Figure S6E), and the IF analysis showed no further accumulation of O^6MeG in p62-KD cells cotreated with TMZ+EPIC-1042 compared to TMZ treatment (Figure 4F). Considering that MGMT was degraded by UPS and p62 KD had no effect on the MGMT level, EPIC-1042-induced increase in p62 binding to PARP1 promoted autophagic degradation of PARP1, which in turn reduced recruitment and poly(ADP)ribosylation of MGMT to enhance TMZ efficacy.

Finally, LN-18 cells were utilized to construct subcutaneous models. We observed that although EPIC-1042 alone did not significantly inhibit tumor growth compared to the DMSO treatment, mice treated with EPIC-1042+TMZ exhibited the smallest tumor burden (Supplementary Figure S7A–D). IHC analysis showed MGMT's expression in LN-18 cells and less Ki-67 in the combination treatment group (Supplementary Figure S7E).

EPIC-1042 Enhances TMZ Sensitivity in Dose-Dependent and Long-Term Treatment Manners in MGMT-Deficient Tumors *In Vivo*

TBD-0220 cell line was utilized to establish an orthotopic GBM model to further validate EPIC-1042's potential in enhancing TMZ efficacy in a dose-dependent manner (Figure 5A). As shown in bioluminescence imaging and OS, compared to TMZ alone group, we observed significant dose-dependent tumor growth inhibition and prolonged survival of EPIC-1042-administered mice when combined with the uniform dose of TMZ (Figure 5B–F). The H&E staining of tumor sections presented similar trend, which was also supported by the Ki-67 staining (Supplementary Figure S8A, Figure 5G). In addition, IHC analysis revealed that in contrast to TMZ alone, PARP1 level started to decrease when TMZ was combined with the lowest dose of EPIC-1042, and the most significant effect was observed in the TMZ with the highest dose of EPIC-1042-treated group (Figure 5G). However, γ-H2AX showed the opposite trend to the PARP1 level, indicating a sign of further damage due to the combination of TMZ with increasing doses of EPIC-1042 (Figure 5G).

Next, administration of TMZ and/or EPIC-1042 (15 mg/kg) for 6 weeks was recapitulated in GBM nude mouse model (Figure 5H). Brain MRI analysis revealed that the TMZ+EPIC-1042 cotreatment group had a relatively lower tumor burden than either the EPIC-1042 or TMZ treatment group (Figure 5I–J). The increase in median survival was reciprocally proportional to the tumor burden, and the combination therapy group exhibited the longest OS benefit (Figure 5K). Collectively, these data implied that EPIC-1042 could enhance TMZ efficacy in dose-dependent and long-term treatment manners.

Preclinical Efficacy of EPIC-1042

To supplement the preclinical data of EPIC-1042, first, the inhibitory effect of EPIC-1042 on various human cytochrome P450 enzymes was evaluated and listed in Supplementary Table S1, and their specific inhibitors were used as the positive control (Figure 6A, Supplementary Figure S9A). EPIC-1042 showed significantly higher IC_{50} for CYP1A2, CYP2C8, CYP2C9, and CYP2E1 than that in the positive control group, indicating less liability for drug–drug interactions with these isozymes. However, for CYP2B6, CYP2C19, and CYP2D6, IC_{50} values were lower than that in the positive control group, suggesting potent inhibition by EPIC-1042 of these isozymes. Interestingly, EPIC-1042 exhibited different trends in IC_{50} values for CYP3A4 when metabolic substrates were different. Next, liver microsomes of mice, rats, dogs, monkeys, and humans were utilized to determine the metabolic stability of EPIC-1042 *in vitro* using clozapine as a positive control (Figure 6B), and the outcomes were listed in Supplementary Table S2. Apart from humans' and monkeys' liver microsomal incubation groups, in which the half-life ($t_{1/2}$) values of EPIC-1042 and clozapine were quite close, the $t_{1/2}$ values of EPIC-1042 were higher than that of clozapine in the other groups, indicating that EPIC-1042 had been quite stable in liver microsomes. Moreover, a manual patch plier assay in HEK293 was carried out to test the cardiotoxicity of EPIC-1042. The IC_{50} of EPIC-1042 was more than 10 μM, which was extremely higher than that of the positive control drug cisapride at 8.068 nM. The result indicated that EPIC-1042 possessed extensively low cardiotoxicity (Figure 6C and Supplementary Figure S9B). Finally, the mean plasma concentration-time profiles of

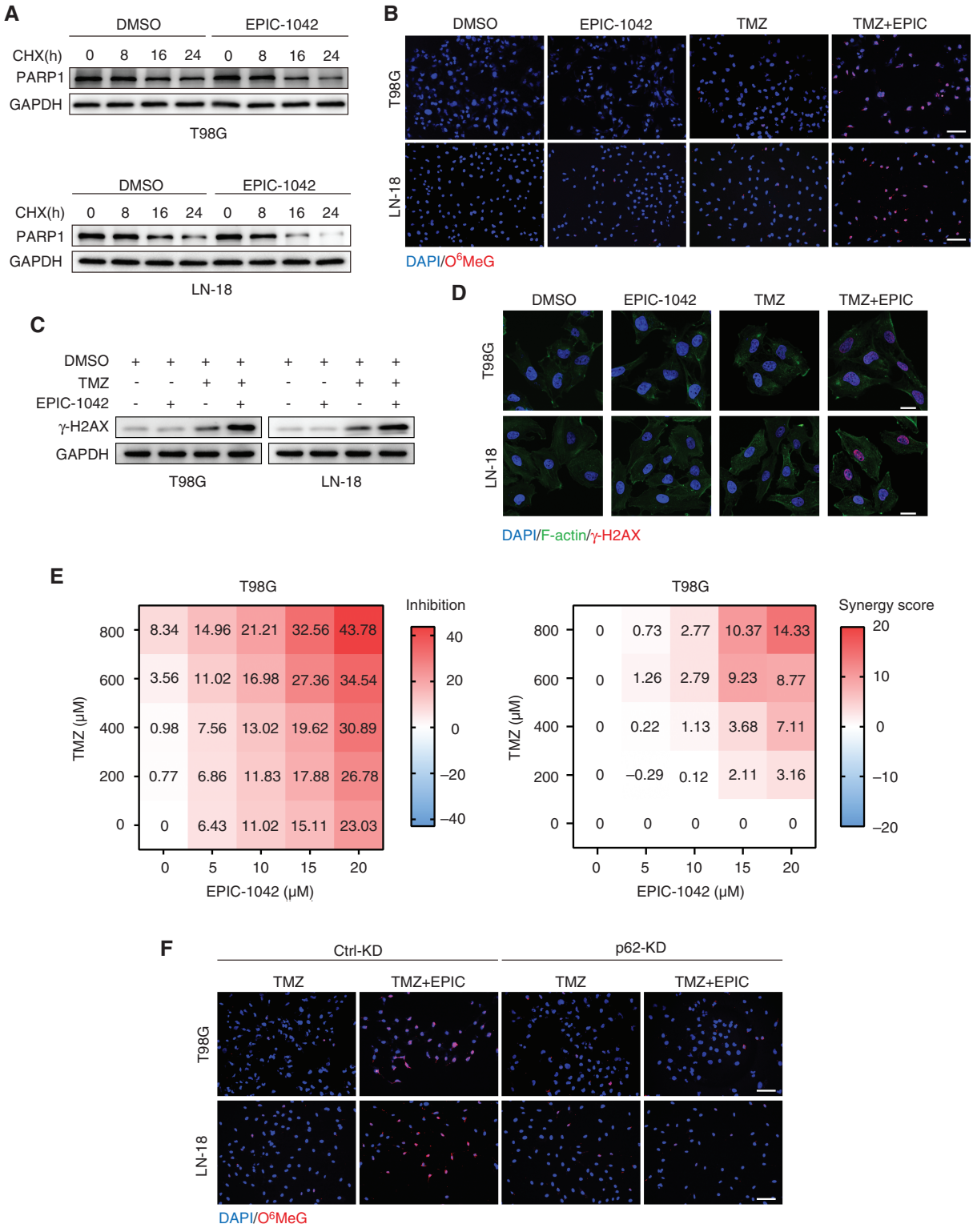

Figure 4. EPIC-1042 enhances TMZ sensitivity in MGMT-positive GBM cells. (A) WB analysis of PARP1 degradation in MGMT-positive cells treated with CHX or combination of CHX with 20 μM of EPIC-1042 for 24 h. (B) IF images of O^6MeG in cells. Scale bar, 100 μm. (C–D) WB analysis and IF images of γ-H2AX in T98G and LN-18 cells. Scale bar, 20 μm. (E) Combination matrices of cell inhibition and synergy scores by EPIC-1042 and TMZ in T98G. Data represent a mean of 3 independent experiments. (F) IF images of O^6MeG in Ctrl-KD and p62-KD cells. Scale bar, 100 μm. In (B–D and F), cells were treated with DMSO, 20 μM of EPIC-1042, 600 μM of TMZ or combination treatment of EPIC-1042 (20 μM) and TMZ (600 μM) for 48 h. Error bars represent mean ± SD; $n = 3$ independent experiments.

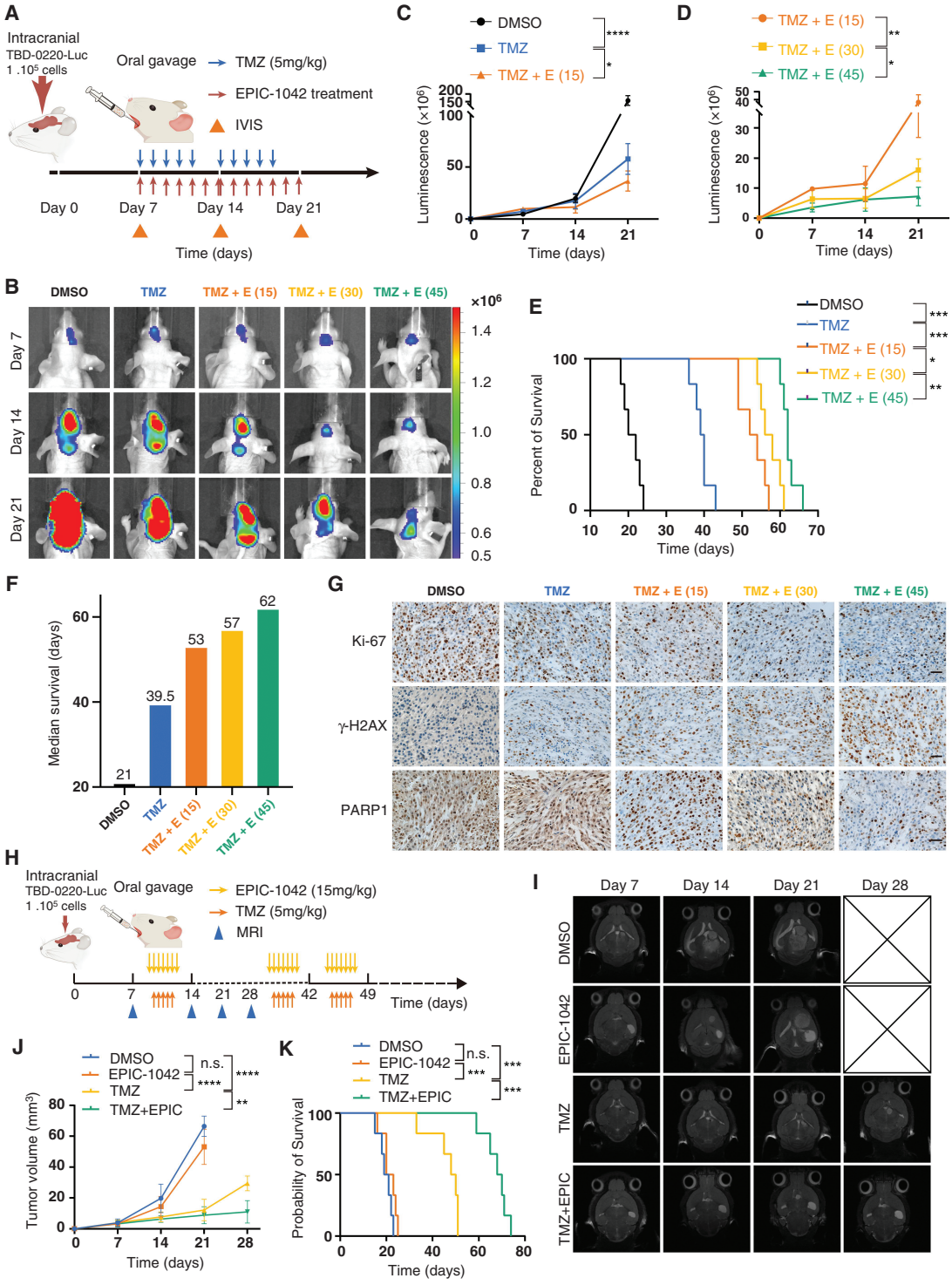

Figure 5. EPIC-1042 enhances TMZ sensitivity in dose-dependent and long-term treatment manners in MGMT-deficient tumors *in vivo*. (A) Tumor-bearing nude mice were treated with DMSO, TMZ (5 mg/kg), or TMZ (5 mg/kg) + EPIC-1042 (15 mg/kg, 30 mg/kg, 45 mg/kg) by gavage for 2 weeks, $n = 6$ for each group. The letter "E" presents EPIC-1042, and the number behind letter "E" stands for the dosage. (B) Bioluminescence images from representative mice of all groups. (C) Quantification of bioluminescence intensity from DMSO-, TMZ (5 mg/kg)- and TMZ (5 mg/kg) + EPIC-1042 (15 mg/kg)-treated groups. *P*, two-way ANOVA. (D) Quantification of bioluminescence intensity from TMZ (5 mg/kg) + EPIC-1042 (15 mg/kg)-, TMZ (5 mg/kg) + EPIC-1042 (30 mg/kg)-, and TMZ (5 mg/kg) + EPIC-1042 (45 mg/kg)-treated groups. *P*, two-way ANOVA. (E) Kaplan–Meier survival curve of nude mice. *P*, Log-rank test. (F) Median survival of all groups. (G) Ki-67, γ-H2AX and PARP1 levels in tumor tissues of all groups. Scale bar, 40 μm. (H) Tumor-bearing nude mice were treated with DMSO, TMZ (5 mg/kg), EPIC-1042 (15 mg/kg), or TMZ (5 mg/kg) + EPIC-1042 (15 mg/kg) by gavage for 6 weeks, $n = 6$ for each group. (I-J) MRI images from representative mice and quantification of tumor size of all groups. *P*, two-way ANOVA. (K) Kaplan–Meier survival curve of nude mice. *P*, Log-rank test. Error bars represent mean ± SD. $^{*}P < 0.05$, $^{**}P < 0.01$, $^{***}P < 0.001$, $^{****}P < 0.0001$, and n.s. indicated no significant difference.

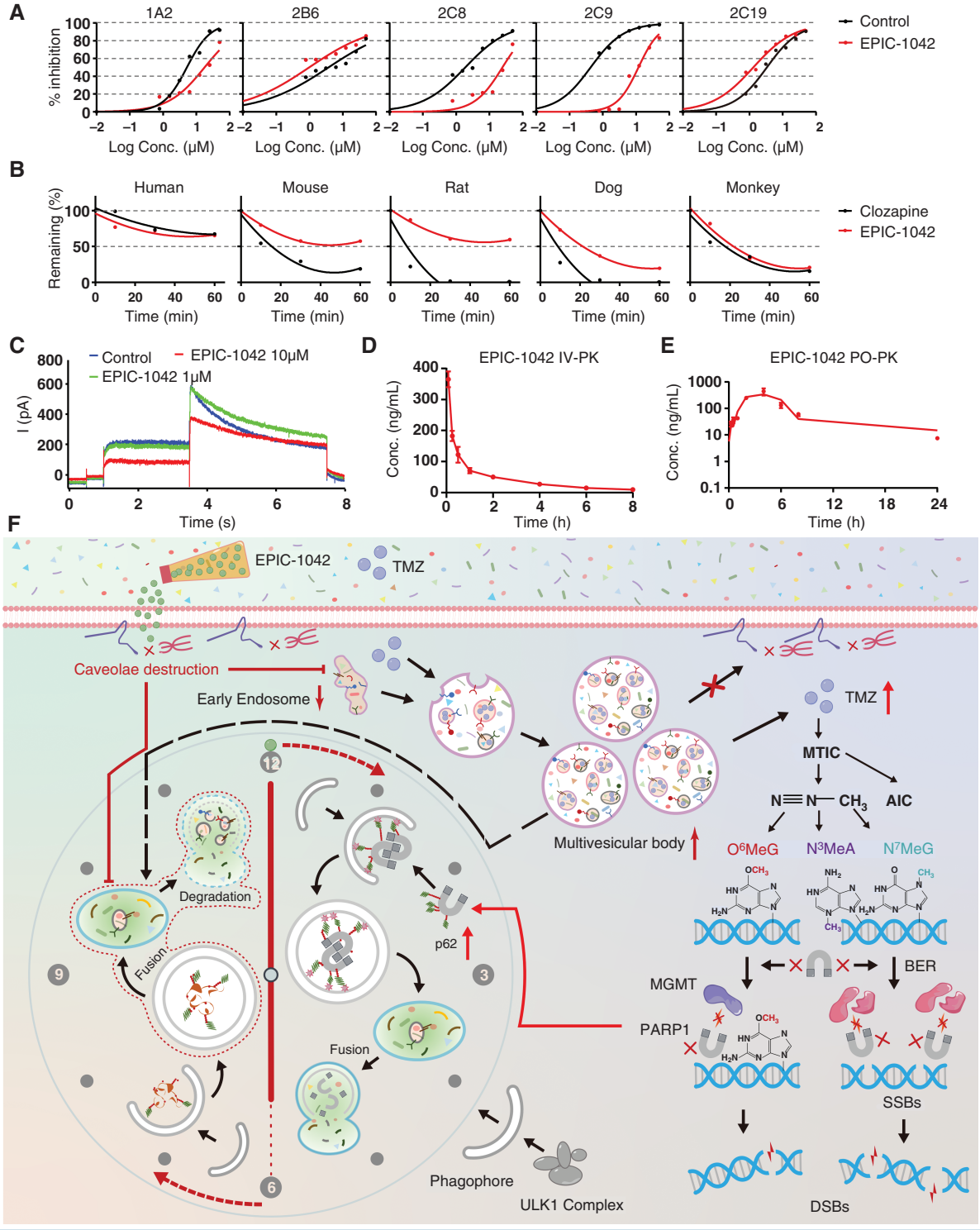

Figure 6. Preclinical efficacy of EPIC-1042. (A) Inhibition of CYP1A2, CYP2B6, CYP2C8, CYP2C9, and CYP2C19 by EPIC-1042 and corresponding positive control drug 7-Ethoxycoumarin, Bupropion, Paclitaxel, Sulfaphenazole, and Omeprazole. (B) Metabolic stability of EPIC-1042 and control drug Clozapine in liver microsomes of humans, mice, rats, dogs, and monkeys. (C) Manual patch plier assay in HEK293 by EPIC-1042. (D–E) Pharmacokinetics of EPIC-1042 in rats at an *i.v.* dose of 2 mg/kg and a *p.o.* dose of 45 mg/kg. (F) Mechanism of action of EPIC-1042.

EPIC-1042 after an *i.v.* dose of 2 mg/kg and a *p.o.* dose of 45 mg/kg were established in a rat model (Figure 6D–E), and the data were available in Supplementary Table S3-4.

To assess the biosafety of EPIC-1042, the nude mice body weights were determined. At the end of fourth week, approximately 5.8% of the body weight of the

TMZ-administrated group was lost compared to the DMSO group. However, there was no significant difference in body weights between the EPIC-1042- and the DMSO-treated groups, and EPIC-1042 did not increase the toxicity of TMZ (Supplementary Figure S9C). No apparent toxicity of the target organs was observed according to the HE staining (Supplementary Figure S9D). The blood routine and the liver and kidney function of the mice were also evaluated while no organ toxicity was found (Supplementary Table S5-6). EPIC-1042 was detected by LC–MS in both tumor and normal brain tissues (Supplementary Figure S9E).

Discussion

In the past few years, many novel therapeutics have been developed to cure GBM, like bevacizumab, erlotinib, immune checkpoint blockade, and irinotecan, but they exhibited limited benefits in clinical trials.[3,25] The FDA approval of TMZ in 2005 exhibited an increase in survival after surgery and radiotherapy from 9–10 months to 14 months.[26] However, TMZ chemoresistance is of growing concern and overcoming that is in urgent need. Furthermore, extensive tumor heterogeneity in GBM suggests that combination therapy can be relatively more effective than monotherapy.

In this study, we characterized the biochemical features of EPIC-1042, targeting the PTRF-CAV1 complex. Streptavidin–biotin pull-down assays showed stable interaction of EPIC-1042 with PTRF, thereby perturbing the association between PTRF and CAV1 as well as intact caveolae, leading to a reduced secretion of sEVs to decrease TMZ efflux and concomitant suppression of autophagic degradation ultimately. Interestingly, in the early stage of treatment, EPIC-1042 increased the p62 level and scarcely inhibited autophagic degradation accompanied by downregulation of PARP1 protein level rather than its mRNA expression. The elevated degradation of PARP1 by EPIC-1042 was mediated by increased binding of p62, resulting in suppressed BER pathway and recruiting of MGMT to repair N^3MeA, N^7MeG, and O^6MeG. In summary, EPIC-1042 decreased sEVs secretion to enhance intracellular TMZ concentration, promoted PARP1 autophagic degradation in the early stage, but inhibited autophagy flux in the end to reverse TMZ chemoresistance.

As shown in the graphics of the predicted simulation (Figure 1B and Supplementary Figure S1D), apart from Glu10 of chain A of PTRF, Tyr7, Asp3 of chain A, Tyr7, Asp3 of chain C and Glu10, Arg11 of chain B with a high degree of conservation were involved and part of them were also involved in the interaction of PTRF and CAV1. Furthermore, Tyr7 of chain A provided potential pi–pi and pi–cation stacking between PTRF and EPIC-1042, which further enhanced their binding.

In this study, we indeed confirmed that disrupting the interaction between PTRF and CAV1 could reduce sEVs production due to the decreased capacity of secretion but not their decreased biogenesis. It has been reported that despite being an integral membrane protein, a portion of CAV1 can be distributed into other organelles, such as endosomes and lysosomes, and can be internalized, which corresponded to our published study that PTRF-CAV1 could be loaded into endocytosis system dependent of caveolae. Furthermore, the cholera enterotoxin B subunit (CTxB) utilizes caveolae to be internalized, demonstrating that lipid rafts exist in the endocytosis system.[20,27] Based on CAV1's important role in lipid raft genesis, there is one possibility that caveolae may generate caveolae-like lipid rafts mimicking physiological caveolae function and containing the PTRF-CAV1 complex via endocytosis. The decreased capacity of sEVs secretion simply due to the blocking of PTRF and CAV1 interaction or decreased caveolae in the membrane and caveolae-like lipid rafts in the endocytosis system needs to be further investigated.

Autophagy, as an important proteolytic system, is an extremely complex cellular process regulated by various factors and contributes to TMZ resistance. We confirmed that EPIC-1042 merely interrupted PTRF-CAV1 association with no change of their protein levels (Figure 1D), leading to increased p62 in the early stage with no influence on the degradation process and cut off the autophagic degradation in the later stage. It was reported that lipid rafts could contain V-ATPase subunits to regulate the acidification process in the lysosomal lumen and disruption of lipid rafts by MBCD may influence lysosome-autophagosome fusion.[20,28] EPIC-1042's effect on autophagy may be due to the destruction of caveolae to prevent caveolae-like lipid rafts genesis and the disruption caveolae-like lipid rafts which had existed in autophagosomes and lysosomes. Moreover, the effect of EPIC-1042 on the autophagy-associated degradation process might be attributed to the blocking of autophagosome-lysosome fusion or the reduction of lysosomal functions, which needs to be further investigated.

PARP1 has been implicated in various DNA repair pathways including the BER pathway and in the maintenance of genomic stability.[29] Illustrating the function of PARP1 in protecting genome integrity is not only vital for designing novel therapeutics but also essential for exploring the underlying mechanisms of chemoresistance in cancers. GPI-15427, a potent inhibitor of PARP1 (80% inhibition in activity), exerts a synergistic effect with TMZ in GBM cells, regardless of the MGMT protein level.[30] In the present study, we found that the PARP1 level was decreased by an increase in p62-mediated autophagic degradation after the administration of EPIC-1042, therefore, impairing BER pathway and recruitment of MGMT. It is reported that PARP1 is normally degraded by UPS[31] which was consistent with our results (Figure 3D), but the Co-IP assays showed that p62 could bind PARP1 under normal conditions (Figure 3G). Apart from being the cargo receptor, p62 also functions as a signal hub and regulates vast signal transduction pathways. For example, p62 can bind ERK1 and negatively regulates the signaling during adipogenesis.[32] Therefore, normally, PARP1 binding with p62 may be required for other signaling pathways apart from autophagic degradations. Moreover, EPIC-1042 might regulate Lys63 (K63)-linked ubiquitin chains possessing a high affinity for p62 during autophagic degradation on PARP1.

In conclusion, our study identified a multifunctional SMI, EPIC-1042, to enhance TMZ efficacy in GBM treatment. With EPIC-1042's mechanisms illustrated and tested *in vitro* and *in vivo*, this study highlighted promising therapeutic strategies using a combination of EPIC-1042 and classical

chemotherapeutics to treat not only GBM but also other cancers.

Supplementary material

Supplementary material is available online at *Neuro-Oncology* (http://neuro-oncology.oxfordjournals.org/).

Keywords

Small-molecular inhibitor |TMZ efflux | Autophagy | PARP1 |TMZ efficacy

Acknowledgements

We thank Shenzhen HUASUAN Technology Co.,Ltd for valuable technical assistance in homology modeling, prediction of interaction patterns, and molecular dynamic simulation.

Conflict of interest statement

The authors declare no competing interests.

Funding

This work was supported by the National Natural Science Foundation of China (NSFC, no. 82272893), the Tianjin Key R&D Plan of Tianjin Science and Technology Plan Project (no. 20YFZCSY00360), and the Key-Area Research and Development Program of Guangdong Province (no. 2023B1111020008).

Author contributions

Conceived the concept and designed the study: CSK and BH. Carried out the experiments: BH, EYY, DYS, JSJ, XTC, QXW, FT, JXZ, SXY, CCC, LX, MLX, KKY, QZ, YQD, HYX and LTC. Analyzed the data, prepared the figures and wrote the manuscript: BH, EYY and DYS. Financially supported and supervised this work: CSK. Approved the final manuscript: All authors.

Data availability

All data generated or analyzed during this study are included in this article, and all data supporting the findings of this study are available from the corresponding author on reasonable request: kang97061@tmu.edu.cn

Affiliations

Department of Neurosurgery, Tianjin Medical University General Hospital, Laboratory of Neuro-oncology, Tianjin Neurological Institute, Key Laboratory of Post-Neuro Injury Neuro-Repair and Regeneration in Central Nervous System, Ministry of Education and Tianjin City, Tianjin, China (B.H., E.Y., D.S., J.J., X.C., Q.W.,F.T., J.Z., S.Y., C.C., Y.D., H.X., L.C., C.K.); Department of Neurosurgery, Affiliated Hospital of Hebei University, Baoding, China (L.X., M.X.); Department of Neuro-Oncology and Neurosurgery, Tianjin Medical University Cancer Institute and Hospital, National Clinical Research Center for Cancer, Key Laboratory of Cancer Prevention and Therapy of Tianjin, Tianjin's Clinical Research Center for Cancer, Tianjin, China (K.Y.); Tianjin Key Laboratory of Composite and Functional Materials, School of Materials Science and Engineering, Tianjin University, Tianjin, China (Q.Z.)

References

1. Lin K, Gueble SE, Sundaram RK, et al. Mechanism-based design of agents that selectively target drug-resistant glioma. *Science*. 2022;377(6605):502–511.
2. Curtin NJ. DNA repair dysregulation from cancer driver to therapeutic target. *Nat Rev Cancer*. 2012;12(12):801–817.
3. Wen PY, Weller M, Lee EQ, et al. Glioblastoma in adults: a Society for Neuro-Oncology (SNO) and European Society of Neuro-Oncology (EANO) consensus review on current management and future directions. *Neuro Oncol*. 2020;22(8):1073–1113.
4. Tomar MS, Kumar A, Srivastava C, Shrivastava A. Elucidating the mechanisms of Temozolomide resistance in gliomas and the strategies to overcome the resistance. *Biochim Biophys Acta Rev Cancer*. 2021;1876(2):188616.
5. Vemula D, Jayasurya P, Sushmitha V, Kumar YN, Bhandari V. CADD, AI and ML in drug discovery: a comprehensive review. *Eur J Pharm Sci*. 2023;181:106324.
6. Poonan P, Agoni C, Ibrahim MAA, Soliman MES. Glioma-targeted therapeutics: computer-aided drug design prospective. *Protein J*. 2021;40(5):601–655.
7. Dantzer F, de La Rubia G, Menissier-De Murcia J, et al. Base excision repair is impaired in mammalian cells lacking Poly(ADP-ribose) polymerase-1. *Biochemistry*. 2000;39(25):7559–7569.
8. Cao X, Lu Y, Liu Y, et al. Combination of PARP inhibitor and temozolomide to suppress chordoma progression. *J Mol Med (Berl)*. 2019;97(8):1183–1193.
9. Hill MM, Bastiani M, Luetterforst R, et al. PTRF-Cavin, a conserved cytoplasmic protein required for caveola formation and function. *Cell*. 2008;132(1):113–124.
10. Chadda R, Mayor S. PTRF triggers a cave in. *Cell*. 2008;132(1):23–24.
11. Bastiani M, Parton RG. Caveolae at a glance. *J Cell Sci*. 2010;123(Pt 22):3831–3836.
12. Wang L, Yang C, Wang Q, et al. Homotrimer cavin1 interacts with caveolin1 to facilitate tumor growth and activate microglia through extracellular vesicles in glioma. *Theranostics*. 2020;10(15):6674–6694.
13. Dong X, Bai X, Ni J, et al. Exosomes and breast cancer drug resistance. *Cell Death Dis*. 2020;11(11):987.
14. Yang E, Wang L, Jin W, et al. PTRF/Cavin-1 enhances chemo-resistance and promotes temozolomide efflux through extracellular vesicles in glioblastoma. *Theranostics*. 2022;12(9):4330–4347.

15. Danieli A, Martens S. p62-mediated phase separation at the intersection of the ubiquitin-proteasome system and autophagy. *J Cell Sci.* 2018;131(19):jcs214304.
16. Huang T, Wan X, Alvarez AA, et al. MIR93 (microRNA -93) regulates tumorigenicity and therapy response of glioblastoma by targeting autophagy. *Autophagy.* 2019;15(6):1100–1111.
17. Hombach-Klonisch S, Mehrpour M, Shojaei S, et al. Glioblastoma and chemoresistance to alkylating agents: Involvement of apoptosis, autophagy, and unfolded protein response. *Pharmacol Ther.* 2018;184:13–41.
18. Li H, Kuang X, Liang L, et al. The beneficial role of Sunitinib in tumor immune surveillance by regulating tumor PD-L1. *Adv Sci (Weinh).* 2021;8(2):2001596.
19. Salle-Teyssieres L, Auclair M, Terro F, et al. Maladaptative autophagy impairs adipose function in congenital generalized lipodystrophy due to Cavin-1 deficiency. *J Clin Endocrinol Metab.* 2016;101(7):2892–2904.
20. Shi Y, Tan SH, Ng S, et al. Critical role of CAV1/caveolin-1 in cell stress responses in human breast cancer cells via modulation of lysosomal function and autophagy. *Autophagy.* 2015;11(5):769–784.
21. Zheng S, Wang W, Aldahdooh J, et al. SynergyFinder plus: toward better interpretation and annotation of drug combination screening datasets. *Genom Proteom Bioinform.* 2022;20(3):587–596.
22. Mahapatra KK, Panigrahi DP, Praharaj PP, et al. Molecular interplay of autophagy and endocytosis in human health and diseases. *Biol Rev Camb Philos Soc.* 2019;94(4):1576–1590.
23. Wu S, Li X, Gao F, et al. PARP-mediated PARylation of MGMT is critical to promote repair of temozolomide-induced O6-methylguanine DNA damage in glioblastoma. *Neuro Oncol.* 2021;23(6):920–931.
24. Murawska GM, Vogel C, Jan M, et al. Repurposing the damage repair protein Methyl guanine Methyl transferase as a ligand inducible fusion Degron. *ACS Chem Biol.* 2022;17(1):24–31.
25. Weller M, van den Bent M, Preusser M, et al. EANO guidelines on the diagnosis and treatment of diffuse gliomas of adulthood. *Nat Rev Clin Oncol.* 2021;18(3):170–186.
26. Janjua TI, Rewatkar P, Ahmed-Cox A, et al. Frontiers in the treatment of glioblastoma: past, present and emerging. *Adv Drug Deliv Rev.* 2021;171:108–138.
27. Dias MVS, Teixeira BL, Rodrigues BR, et al. PRNP/prion protein regulates the secretion of exosomes modulating CAV1/caveolin-1-suppressed autophagy. *Autophagy.* 2016;12(11):2113–2128.
28. Yoshinaka K, Kumanogoh H, Nakamura S, Maekawa S. Identification of V-ATPase as a major component in the raft fraction prepared from the synaptic plasma membrane and the synaptic vesicle of rat brain. *Neurosci Lett.* 2004;363(2):168–172.
29. Ray Chaudhuri A, Nussenzweig A. The multifaceted roles of PARP1 in DNA repair and chromatin remodelling. *Nat Rev Mol Cell Biol.* 2017;18(10):610–621.
30. Tentori L, Ricci-Vitiani L, Muzi A, et al. Pharmacological inhibition of poly(ADP-ribose) polymerase-1 modulates resistance of human glioblastoma stem cells to temozolomide. *BMC Cancer.* 2014;14(1):151.
31. Zhang N, Zhang Y, Qian H, et al. Selective targeting of ubiquitination and degradation of PARP1 by E3 ubiquitin ligase WWP2 regulates isoproterenol-induced cardiac remodeling. *Cell Death Differ.* 2020;27(9):2605–2619.
32. Komatsu M, Kageyama S, Ichimura Y. p62/SQSTM1/A170: physiology and pathology. *Pharmacol Res.* 2012;66(6):457–462.